



**HAL**  
open science

# Experimental study of foam propagation and stability in highly permeable porous media under lateral water flow: Diverting groundwater for application to soil remediation

Hossein Davarzani, Romain Aranda, Stéfan Colombano, Fabien Laurent,  
Henri Bertin

## ► To cite this version:

Hossein Davarzani, Romain Aranda, Stéfan Colombano, Fabien Laurent, Henri Bertin. Experimental study of foam propagation and stability in highly permeable porous media under lateral water flow: Diverting groundwater for application to soil remediation. *Journal of Contaminant Hydrology*, 2021, 243, pp.103917. 10.1016/j.jconhyd.2021.103917 . hal-03498840

**HAL Id: hal-03498840**

**<https://hal.science/hal-03498840>**

Submitted on 5 Jan 2024

**HAL** is a multi-disciplinary open access archive for the deposit and dissemination of scientific research documents, whether they are published or not. The documents may come from teaching and research institutions in France or abroad, or from public or private research centers.

L'archive ouverte pluridisciplinaire **HAL**, est destinée au dépôt et à la diffusion de documents scientifiques de niveau recherche, publiés ou non, émanant des établissements d'enseignement et de recherche français ou étrangers, des laboratoires publics ou privés.



Distributed under a Creative Commons Attribution - NonCommercial 4.0 International License

## **Experimental study of foam propagation and stability in highly permeable porous media under lateral water flow: diverting groundwater for application to soil remediation**

Hossein Davarzani<sup>a</sup>, Romain Aranda<sup>a</sup>, Stéfan Colombano<sup>a</sup>, Fabien Laurent<sup>c</sup>, Henri Bertin<sup>b</sup>

a: BRGM, 3 Avenue Claude Guillemin, 45100, Orléans, France.

b: I2M, Université de Bordeaux, 33405, Talence, France.

c: Solvay RICL, 85 rue des Frères Perret, 69192, St Fons, France.

Email: h.davarzani@brgm.fr. Phone : +33 (0)2 38 64 33 52.

### **Abstract**

Foam propagation and stability in highly permeable porous media, encountered in soil pollution applications, are still challenging. Here, we investigated the application of foam for blocking the aquifer to divert the flow from a contaminated zone and, therefore, ease the remediation treatments. The main aim was to better understand the critical parameters when the foam is injected into a highly permeable aquifer with high groundwater flow velocity (up to 10 m/day). A decimetric-scale 2D tank experimental setup filled with 1 mm glass beads was used. The front part of the 2D tank was made of transparent glass to photograph the foam flow using the light-reflected method. The water flow was generated horizontally through injection and pumping points on the sides of the tank. The pre-generated foam was injected at the bottom center of the tank. Water streamlines (using dye tracing) and water saturation were investigated using image interpretation. Results show that 100% of the water flow was diverted during the injection of the foam. Foam stability in porous media depends significantly on the horizontal water flow rate. Recirculating water containing the surfactant increases foam stability. The main mechanism of destruction was identified as the dilution of the surfactant in water. However, the head-loss measurements showed that despite foam destruction, the relative permeability of the water phase in the media remained quite low. Injection of foam increases the radius of gas propagation, thanks to foam's high viscosity, compared to a pure gas injection case. These results are new highlights on the efficiency of foam as a blocking agent, showing that it can also serve as a means for gas transport more efficiently in porous media, especially for soil remediation applications.

## **Keywords**

Foam, saturated zone, soil pollution, high permeability, 2D tank

## **Highlights**

- Foam can efficiently divert lateral water flow in highly permeable porous media
- High gas saturation after foam destruction leads to reduce the mobility
- Lateral flow velocity significantly affects foam stability
- Recirculation of water containing the surfactant increases foam stability

## **1. Introduction**

Foams have multiple applications in soil remediation. In recent research, three different foam uses were studied: vectorization, desorption and mobilization, and blocking foams. For each foam technology, new formulations must be considered (surfactant and its concentration, additives, gas) to adjust the properties of the foam to its application. Vectorization foam is used to transport a specific additive for an in situ chemical remediation. Foams can transport nanoparticles [Sheng, 2013], calcium polysulfide [Zhong et al., 2011], bacteria for aerobic biodegradation [Choi et al., 2009], or hydrogen [Maire et al., 2019]. Desorption and mobilization foams use the surfactant properties of the foam to desorb pollutants and push them to a recovery well. Recent laboratory studies have been carried out to assess how foam behaves in porous media for shallow contaminated soil remediation [Couto et al., 2009; Dickson et al., 2002; Mulligan and Eftekhari, 2003]. Several studies have focused on the remediation of soils contaminated by DNAPL, such as trichloroethylene (TCE) [Jeong and Corapcioglu, 2003; Jeong et al., 2000; Rothmel et al., 1998].

Foam as blocking or diverting agents acts to reduce fluid flow in a high permeability zone of heterogeneous porous media. This blocking effect is possible thanks to the high viscosity of the foam and its gas fraction, reducing the mobility of water in the injected area. Foams formed in the different layers of soil are not identical; in general, stronger foam is generated in the layers of higher permeability, partially blocking these layers. This helps to homogenize flows between different layers. This is one of the main advantages of foam as a non-Newtonian fluid. A few authors have studied foam in the laboratory with the objective of a blocking application [Aranda et al., 2020; Bertin et al., 2017; Kavscek and Bertin, 2003; Portois et al., 2018a; Portois et al., 2018b]. Blocking more permeable areas also redirects recovery fluids to less permeable areas [Wever et al., 2011]. The reason is related to bubble stability and the capillary pressure

[Khatib et al., 1988]. Layers with high permeabilities have larger pores and therefore lower capillary pressure. Low capillary pressure means that the foam bubbles will not break as easily in these layers. In addition, small bubbles in more permeable layers will reduce gas mobility and divert the flow of water in these layers [Rossen et al., 1999]. The foam generated for blocking applications must be very stable to withstand flow over potentially long periods. The main phenomenon for foam coalescence in porous media is related to the capillary pressure introduced generally as a critical value [Kovscek et al., 2007]. The capillary pressure in porous media is a function of water saturation and surfactant concentration. Surfactant concentration, as well as foam quality, also significantly influence foam stability in porous media [Wang and Mulligan, 2004].

More recently, Aranda et al. (2020) investigated the properties of foam generated using an alpha-olefin sulfonate surfactant and nitrogen for flow-blocking purposes in a very high permeable porous medium ( $> 10^{-10} \text{ m}^2$ ). A packed column was used to study the impact of different parameters such as the foam generation method and the pre-generated foam permeability on the foam blocking properties. Foam flow in highly porous media behaves with two regimes: a weak foam flow followed by a strong foam flow. These two distinct flow regimes were more significant when the foam was generated by the co-injection technique (surfactant and gas). They found that a pre-generated foam is a good option for blocking the highly permeable zone. This pre-generated foam showed non-Newtonian, shear-thinning behavior [Aranda et al., 2020; Omirbekov et al., 2020a; Omirbekov et al., 2020b].

The final goal of this study was not to redirect the groundwater flows in areas of low permeability but rather to block an entire area upstream of the area to be remedied. The final goal was to divert or slow down underground flows and to isolate the saturated zone which is under chemical treatment (Fig. 1). The increase in the residence time inside this zone should facilitate the implementation of in situ remediation techniques in the saturated zone (chemical vectorization and treatments). At the end of the remediation processes, the foam will have to be destroyed naturally to allow underground flows naturally. Finally, the pilot site on which these technologies will potentially be applied has very high permeability (from  $10^{-10}$  to  $10^{-8} \text{ m}^2$ ). Thus, one of the main novelties of the present work is to study the blocking effect of foam in highly permeable porous media.

At the microscopic scale, foam has been studied in micro-models to examine the generation and destruction of gas bubbles through their direct visualization and thus establish a predictive

model of bubble size distribution in the foam [Géraud et al., 2017]. On a macroscopic scale, foam flow has been studied in homogeneous and heterogeneous media. Foam propagation in 2D tanks has been studied recently by some authors [Bertin et al., 2017; Bouzid et al., 2018; Forey et al., 2021; Longpré-Girard et al., 2016] using different configurations to focus on the effect of heterogeneity and/or the presence of pollutant. They showed the importance of several physical parameters like permeability contrast, presence of pollutant, and surfactant formulation on the foam propagation and stability. To our knowledge, there is a lack of information in the literature concerning the study of foam flow and stability under water flow conditions in a decimetric-scale 2D setup.

The setup presented here combines dye tracing, mass balance calculation, and a photographic analysis technique to assess foam flow and saturation values in the porous medium.

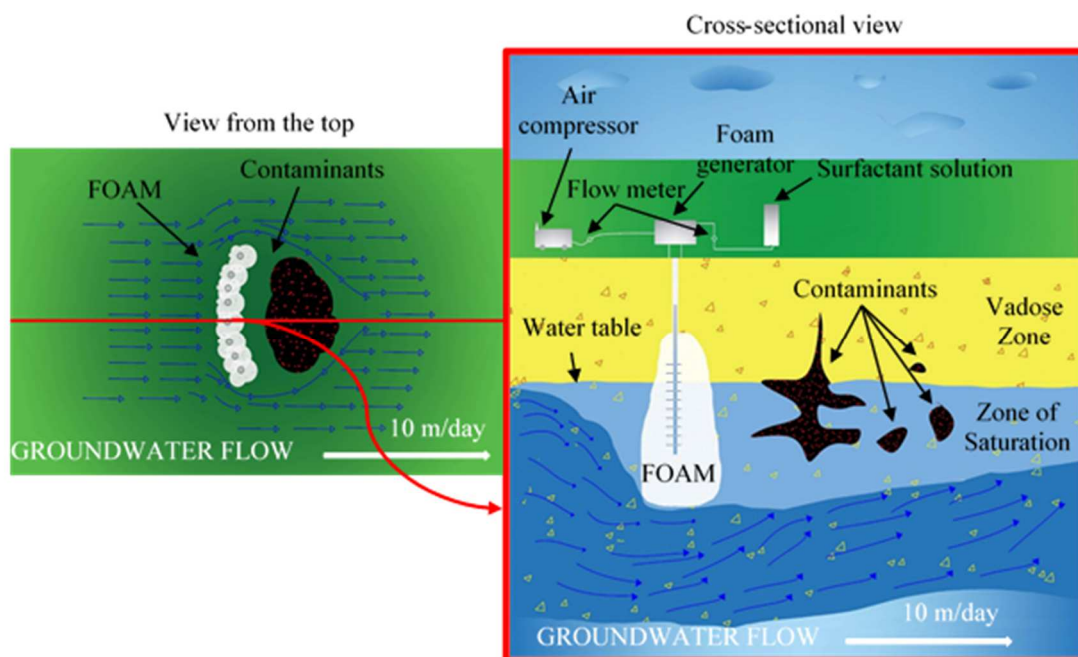


*Fig. 1. Schematic illustration of the foam injection process for groundwater flow diverting*

The objective of the present research work was to study foam injection in the presence of a flow of water to assess its potential as a blocking fluid for diverting flow from a polluted area. Although the real situation occurs in a 3D geometry, to simplify the problem and to visualize better the foam flow using an imaging technique, all experiments were carried out in a 2D tank. The propagation and the stability of the foam were studied in a reference case with a water flow of different velocities, as well as 10 m/day, according to the groundwater flow rate in a real

polluted site. Additional experiments were carried out to study the influence of the nature of the water flow and its velocity on the propagation and stability of the foam.

## **2. Materials and fluids**

### **2.1. Porous media**

In all 2D tank experiments, 1 mm glass beads were used for the study. These glass beads, supplied by Dutscher<sup>®</sup>, were the same as those used in [Aranda et al., 2020; Omirbekov et al., 2020b]. The porous media obtained using these glass beads have an average permeability of  $8.4 \times 10^{-10} \text{ m}^2$  and an average porosity of 0.37. The transparency properties of glass beads allow good visualization of flows and saturation levels by image analysis.

### **2.2. Surfactant solution and gas**

Building upon the results in [Aranda et al., 2020; Omirbekov et al., 2020b], a solution of alpha-olefin sulfonate surfactant (AOS) concentrated at  $4 \times \text{CMC}$  was used for the experiments. The surfactant solutions were always prepared the same day or the day before starting the experiments to avoid possible aging effects. In addition, further surface tension measurements were made on the stock solution to ensure that the CMC value (1.8 g/L) had not changed over time. The results show that the CMC was not changed for more than a year after opening the product. The gas used to generate the foam was  $\text{N}_2$  supplied by Air Liquide<sup>®</sup> (purity > 99.99%). Carbon dioxide, supplied by the same provider (purity > 99.7%), was also used to prepare the foam pre-generator.

## **3. Experimental setup and procedure**

### **3.1. Foam pre-generation**

The pre-generator consists of a porous medium made of calibrated glass beads of 0.1 mm diameter contained in a PVC column of 10 cm effective length as presented in (Aranda et al., 2020). The porous medium porosity of the pre-generator column was 0.38 with a permeability of  $1.1 \times 10^{-11} \text{ m}^2$ .

### **3.2. 2D tank setup**

Two tanks of small (S) and medium (M) sizes were used in this study. The geometric characteristics of the porous media contained in these tanks are presented in Table 1. 2D tanks are composed of a central volume to contain the porous medium. On the two sides of this volume are two cavities separated from the central volume by two 250  $\mu\text{m}$  metal grids allowing fluids to flow but fine enough to contain the porous medium. The cavities insure an almost

vertical homogeneous pressure inside the 2D tank. The dimensions of 2D tank and the length of the cavities are specified in Table 1. The assumption was made that the flows in the tanks were two-dimensional. To support this hypothesis, the ratios between the effective height of the saturated porous medium and its width are also presented in Table 1. The tanks have a central injection point on their lower part through which the foam is injected. The M tank also has side connection points for connecting pipes and generating lateral water flows.

*Table 1. Characteristics of the porous medium contained in the different tanks.*

2D tank	Effective length $l$ [cm]	Total height $H$ [cm]	Saturated height $h$ [cm]	Tank width $e$ [cm]	$e/h$	Cavity length $l_c$ [cm]
Small (S)	43.5	25	20	2.2	0.11	2.0
Medium (M)	51.0	35	30	4.0	0.13	1.8

The experimental setup is presented in Fig. 2. It consists of a primary circuit (foam injection), a secondary circuit (lateral flow of water), and a tertiary circuit (pumping of excess water). In the primary circuit, the nitrogen and the surfactant solution are co-injected into the foam pre-generator column, the gas using a Brooks<sup>®</sup> Delta Smart II mass flowmeter (precision:  $\pm 0.34 \text{ mL}\cdot\text{min}^{-1}$ ), and the liquid by an Ismatec<sup>®</sup> Reglo ICC peristaltic pump (precision:  $\pm 0.063 \text{ mL}\cdot\text{min}^{-1}$ ). The co-injection system used a Swagelok<sup>®</sup> Tee connector. The fluids left the pre-generator in the form of foam. This foam flowed to a 4-way valve which directed it either to a beaker while awaiting stabilization, or to the tank to begin injection. The circuit pipes were made of PVC and had an inside diameter of 0.635 cm.

The secondary circuit consisted of four pipes and an Ismatec<sup>®</sup> Reglo ICC peristaltic pump with four independent channels. This circuit allows deionized water to be injected into the inlet (or left) cavity of the tank. This injection was carried out by two pipes, the ends of which were located at the top and bottom of the cavity (S tank) or at two lateral connection points (M tank) to create as homogeneous a flow as possible. Likewise, two pipes pumped water from the outlet (or right) cavity, symmetrically to the water injection pipes. To maintain a constant lateral flow, the pumping rate in all four pipes was the same. The tertiary circuit was made up of two pipes and an Ismatec<sup>®</sup> Reglo ICC peristaltic pump. The two ends of the pipes were placed at the water/air interface in the two cavities, directly in the cavity (S tank) or attached to a connection point (M tank). This circuit was used to pump excess water from the cavities. When foam was injected into the tank, it occupied a volume replacing water that should be pumped by the

tertiary circuit to a beaker placed on a Sartorius<sup>®</sup> MSE8201S balance (precision:  $\pm 0.1$  g). From the measured mass, one can deduce the volume occupied by the foam during the injection.

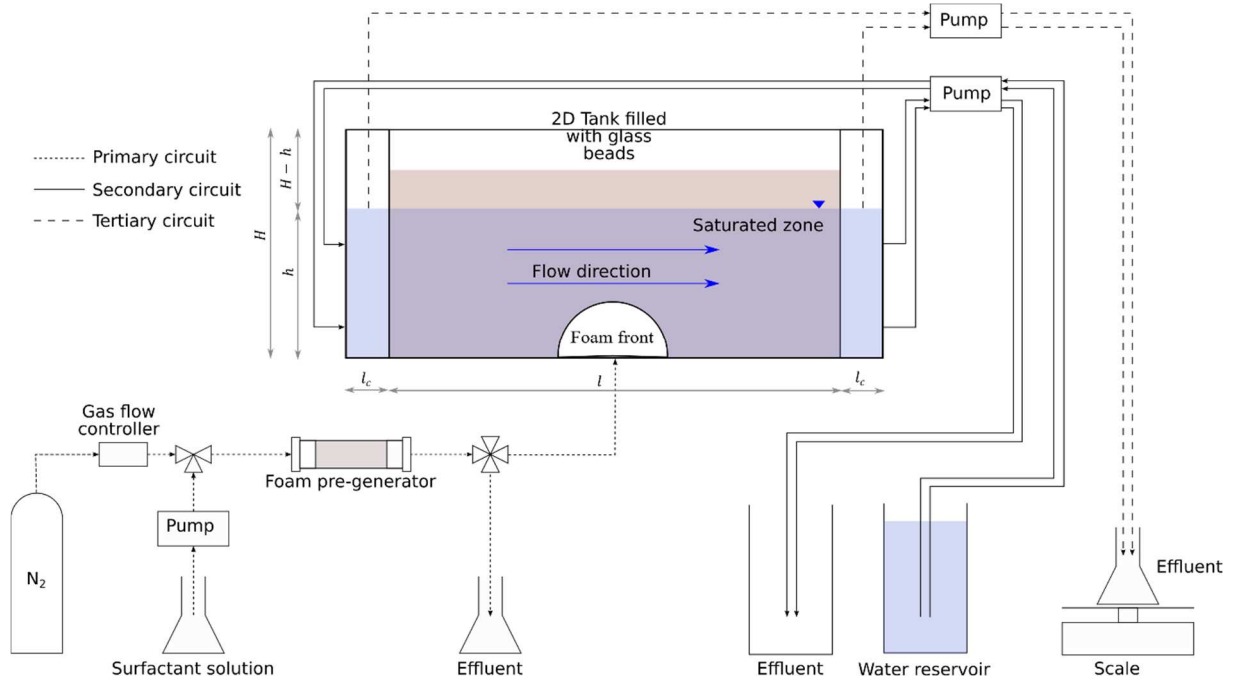


Fig. 2. Experimental 2D tank setup for foam injection and stability study. 2D tank was filled with 1 mm glass beads. The water flows horizontally and pre-generated foam is injected from a bottom center hole (small tank dimensions:  $l=43.5$  cm,  $H=25$  cm,  $h=20$  cm and  $l_c=2$  cm; medium tank dimensions:  $l=51$  cm,  $H=35$  cm,  $h=30$  cm and  $l_c=1.8$  cm).

Photos were taken using a Nikon<sup>®</sup> D850 camera with a 105 mm focal length lens installed on a tripod. The camera was placed in the central axis of the tank, as close as possible but at sufficient distance to capture the entire tank. A Broncolor<sup>®</sup> Litos projector was placed above the tank, slightly in front of the device, and off-center. The placement above the tank avoids the reflection of the projector on the 2D tank glass. The slight offset ensured that images were not obstructed by the projector foot. A Squadra XpoGrey<sup>®</sup> element representing standard gray levels was attached to the tank to allow the photographs to be calibrated. During the first photography tests, these standards served to verify that white was not overexposed (brightness value = 255) or underexposed black (brightness value = 0). The photos were taken in a darkroom to overcome variations in exterior light.

### 3.3. Experimental procedures

The 2D tanks were slowly filled up to height  $H$  with glass beads to obtain a homogeneous stack. Deionized water was then injected through the injection point at the bottom of the tank



at a rate of 2.0 mL/min. The homogeneity of the glass beads and the low injection speed keep water flow stable. Due to very low capillary effects, no air bubbles trapped in the medium were observed. The tank was saturated with water up to an effective saturated height  $h$  listed in Table 1 and shown in Fig. 2. The unsaturated zone helps to prevent the lateral flow of water at the surface. All experiments are referenced in Table 2 with the size of the associated tank and the type of lateral flow.

The type of lateral flow was changed in some experiments. The lateral flow is of type “open” when the deionized water is injected continuously. The experimental setup has been modified so that the pipes of the secondary flow operate in a closed circuit. This means that the fluid pumped into the outlet cavity is directly reinjected into the inlet cavity (instead of deionized water). A flow of this “closed” type allows water to be reused in the tank with a surfactant that has been diluted beforehand and carried away by the lateral flow. Finally, some experiments were simply carried out without activating the secondary circuit. In this case, there is no lateral flow in the tank (“without flow” case). This corresponds to the ideal case where there is no groundwater flow and foam should be in its maximum stability value. It can help to better understand the effect of the lateral flow on foam flow behavior which is one of the main objectives of this work.

*Table 2. Summary of the experiments carried out in the 2D tank.*

Experiment number	2D tank	Lateral water flow type	Lateral flow velocity
1	S	Open	10 m/day
2	S	Without flow	-
3	S	Closed	10 m/day
4	M	Open	5 m/day
5	M	Open	7.5 m/day
6	M	Open	10 m/day
7	M	Without flow	-

The pre-generator column was first filled with the porous medium (0.1 mm glass beads). Then CO<sub>2</sub> was injected into the column followed by deionized water, and finally the AOS surfactant solution at a concentration of 4×CMC. Since a pre-generator column is used for several experiments, it is initially filled with destroyed foam (gas and surfactant solution) as the experiment is initialized.

Following the same procedures as described in [Aranda et al., 2020], gas and surfactant solution are co-injected into the pre-generator directing the foam to the effluent beaker using the 4-way valve. This achieves a steady-state foam flow in the pre-generator column guaranteeing that the foam quality is 85% and the total flow rate is 4 mL/min. The objective of this preliminary step is to generate a strong foam repeatable for each experiment inside the pre-generator. The steady-state was achieved when the pressure signal before the pre-generator became stable. At the same time, the second circuit was activated to generate a lateral flow with a flow velocity of 10 m/day. The tertiary circuit was also activated to pump out any water excess before the start of the experiment. To confirm the homogeneity of the lateral flow, a tracing test was carried out with a solution of bromocresol green (BCG) at 1 g.L<sup>-1</sup>. The dye is injected into the inlet left cavity and its flow is photographed. Finally, when all the flows are stable and the foam is ready to be injected, a first (zero) photo is taken. The foam was injected into the 2D tank by changing the 4-way valve. At the end of the injection period, the 4-way valve was turned to direct the foam to the effluent beaker. The primary circuit (injection) was stopped but the secondary and tertiary circuits were left active to study the stability of the foam over time. A new tracing is done at the end of the experiment to visualize the impact of the foam on the lateral flow. The duration of the injection was not the same for all the experiments. Some injections had to be stopped earlier because of some experimental constraints.

#### **4. Image Analysis**

To use the data acquired by photography, the images must be processed and interpreted. The final objective of this approach is to define a relationship between light intensity and liquid saturation. To achieve this, we used the light reflection methods (LRM) (see [Alazaiza et al., 2016]).

##### **4.1. Image treatments**

First, a global area of interest (AOI) was defined to obtain the mean grey value necessary to associate with the water saturation. This area is smaller than the 2D tank glass surface to remove the shadows that appear near the edges. Before any treatment step, it is important to choose the appropriate analyzing wavelength. The authors recommend working in monochrome [Flores et al., 2011]; however, the technical limitations in the laboratory made it necessary to use white light during the experiments. As the foam is white, its intensity is approximately equal in all monochrome spectra. Consequently, the choice was made to work on shades of gray. The photographs are therefore converted into a 8-bit format to obtain 255 shades of grey. The gray level was calculated using  $I_{grey} = (I_{red} + I_{green} + I_{blue})/3$  where  $I$  is the light intensity (-),

between 0 and 255. There are many other methods described in the literature for converting RGB color images to grayscale [Câdık, 2008]. The most appropriate technique should be chosen according to the set objective (aesthetics, contrast, highlighting a particular color, etc.).

Many pixels may have under or over brightening. To correct this effect, it is essential to create small meshes where the intensity of the pixels will be averaged. The first step is to determine the optimal size of this mesh. For simplicity, these meshes will be square. The optimal size should be chosen as small as possible to get the most accurate information possible, but large enough to avoid pixel order variations. The primary analysis showed that the microscopic variations in intensity stabilize at an area of 8,836 px<sup>2</sup>, or a small mesh of 94 pixels per side.

In the photographs, the lighting may also not be perfectly uniform in the horizontal and vertical directions. To correct this lack of uniformity, the global mean intensity  $I_m$  over AOI is calculated on an image before injecting foam (reference image) where the 2D tank is fully saturated with water  $S_l = 1$  ( $t = 0$ ). Each analysis of a series (for one experiment) of photos will be based on its reference image. The matrix  $\Delta I_0$  is defined for each mesh such that  $\Delta I_0 = I_m - I_{raw}$  with  $I_{raw}$  the mean intensity over each small mesh. This uniformization gives a unified gray corresponding to  $S_l = 1$ . However, the difference  $\Delta I_0$  between the global average value  $I_m$  over AOI and the original average value of each small mesh  $I_{raw}$  is kept for the rest of the analysis.

Finally, the intensity is linearly corrected using the standard black and white of the image

$$I = 255 \left( \frac{I_{uni} - I_{black}}{I_{white} - I_{black}} \right) \quad (1)$$

where  $I$  is the corrected intensity of each small mesh. The coefficient 255 changes the value of the intensity to a scale of 0 to 255 as initially to obtain more meaningful values. Technically, this coefficient is unnecessary for image analysis.  $I_{white}$  and  $I_{black}$  are the standard white and black intensities of the analyzed image, and  $I_{uni}$  the uniform intensity of each mesh is calculated as below using the variations in the intensity of the image zero  $\Delta I_0$ .

$$I_{uni} = I_{raw} + \lambda \Delta I_0 \quad (2)$$

where  $\lambda(-)$  presents the correction for the possible variation between photographs

$$\lambda = \frac{I_{white} - I_{black}}{I_{0,white} - I_{0,black}} \quad (3)$$

where  $I_{0,white}$  and  $I_{0,black}$  are the standard black and white intensities of the image zero.

#### 4.2. Calibration of the intensity-saturation relationship

The optical density was used to estimate water saturation from grayscale images of a 2D tank [Flores et al., 2011; Kechavarzi et al., 2000]. It has been shown that the optical density can be related to water saturation using a linear function [Colombano et al., 2020; Luciano et al., 2010; O'Carroll et al., 2004; Philippe et al., 2020]. In the case of light reflection methods, the transmitted and received energy flux can be associated with the measured reflected light intensity  $I_r$ , and the light intensity reflected by a perfect white surface  $I_i$  [Flores et al., 2011; Kechavarzi et al., 2000; Schincariol et al., 1993]. Therefore, the optical density ( $OD$ ) can be calculated as

$$OD = -\log_{10} \left( \frac{I_r}{I_i} \right) \quad (4)$$

Then the water saturation can be calculated according to a linear relationship

$$S_l = \alpha OD + \beta \quad (5)$$

The coefficients  $\alpha$  and  $\beta$  are then calculated from two calibration images where the saturations are known. For high precision and simplicity, the photos used were at  $S_l = 0.15$  (value of liquid saturation in the foam just after injection) and  $S_l = 1$ . To visualize the results of this analysis, the meshes were colored according to their gray intensity. This visualization imposes a discretization of intensities and saturations. For this study, the saturation slices [0; 0.1], [0.1; 0.3], [0.3; 0.5], [0.5; 0.7], [0.7; 0.9], [0.9; 1] were used and associated with a color scale from white to blue.

#### 4.3. Method validation

To validate this method, the volume of gas in the tank calculated from the image analysis was compared to that calculated from the mass measurements of the excess water. For this comparison, an experiment without lateral flow was used to eliminate errors due to a difference between the injection and pumping rates generating the lateral injection. During injection, the gas occupied a volume equal to the volume of water leaving the tank from which the volume of injected surfactant solution is subtracted. From imaging, the volume of gas in the tank was deduced from the saturation values calculated from the light intensity considering the 2D tank

volume and porous medium porosity. The calibration performed on this experiment gave the values  $\alpha = -2.90$ ,  $\beta = 6.40$  and  $I_m = 70$ .

Fig. 3 presents the temporal evolution of the volume of gas in the tank, calculated by measuring the mass and estimated by imaging. Error bars represent 5% of the value calculated by imaging. The values calculated by the two techniques are similar within only 5% of error. It is therefore concluded that the imaging analysis technique allows estimation of the saturation in the tank within  $\pm 5\%$ .

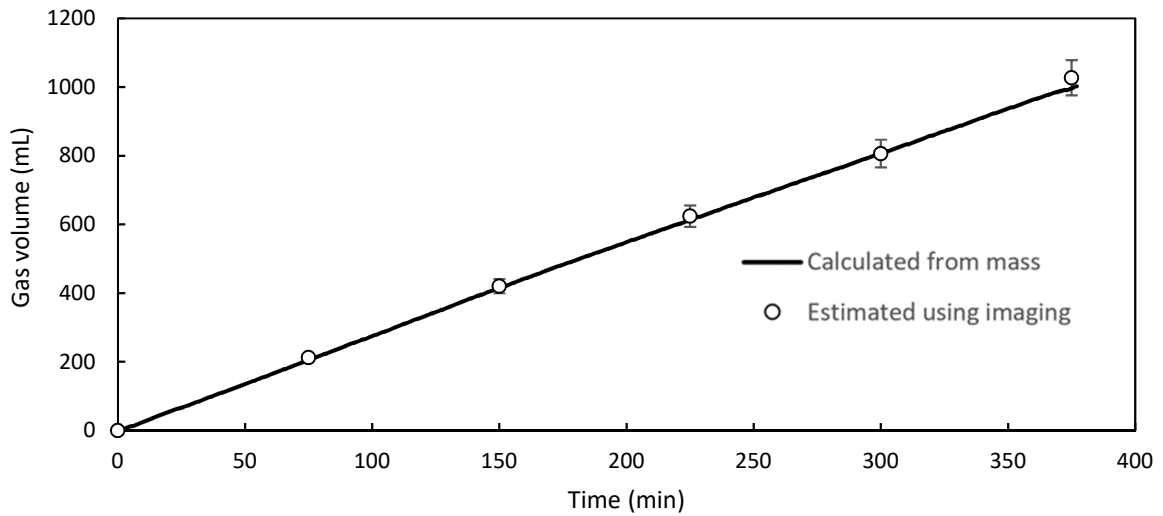


Fig. 3. Gas volume in the tank as a function of time, calculated by mass measurement and estimated by imaging. Error bars represent 5% of the value calculated by imaging.

## 5. Results and Discussions

### 5.1. Foam flow and its blocking effect

This section discusses the results obtained for the reference case (lateral flow of 10 m/day), i.e., the propagation of the foam front, the ability to block the lateral flow, and the stability of the foam in the porous medium after stopping the injection.

Fig. 4 shows the results of the tracings carried out before and after injection into the S tank (experiment #1). Before injection, the tracer flows quite uniformly across the 2D tank. The broadening of the shape is due to the diffusion of the tracer in the porous medium. After the foam injection is complete, the tracer flows around the strong foam. The lateral flow of water is therefore completely diverted by the strong foam. In this case, the foam injection was extended so that it reached the unsaturated zone of the tank. The photos show that the water level rises upstream to allow water to flow over the foam.

This behavior is attributed to low mobility of strong foam due to its high viscosity and low relative permeability. Therefore, water flows around the foam zone as seen in Fig. 4. These results demonstrate that the foam can divert the flow of water, acting as a blocking fluid.

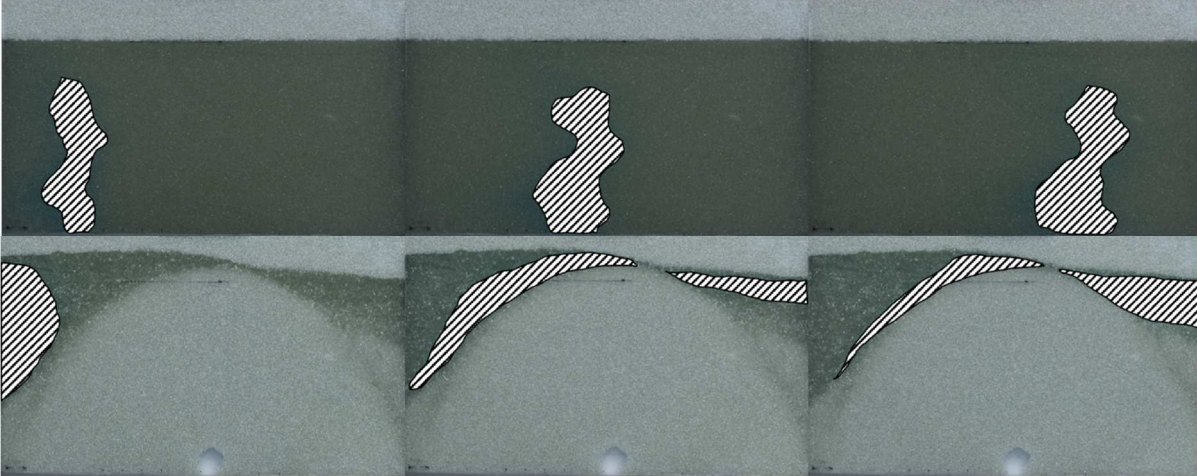


Fig. 4. Traces before and after injection of foam. The tracer is identified by the hatched area. 2D tank S (# 1). Top: Before injection (15 minutes between each photo). Bottom: After injection (5 minutes between each photo).

**5.2. Stability**

After the end of the foam injection, its temporal stability was investigated. During this phase of the experiment, a lateral water flow was maintained in the tank. Fig. 5’s photos show the destruction of the foam in the tank M (experiment #6) during the stability phase. The strong foam is weakened progressively and destroyed after 53 hours of constant water flow. Shortly after this stage of foam destruction, the gas phase was redistributed in the whole 2D tank. Most of the remaining gas in the porous medium was then trapped by capillary forces in the pores.

Time (h)	Foam evolution	Time (h)	Foam evolution
0		10	

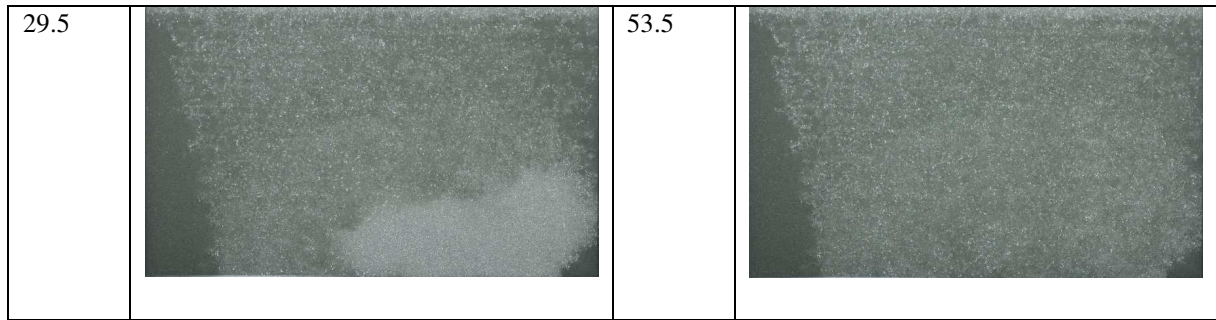


Fig. 5. Time evolution of the foam zone submitted to a lateral water flow ( $V = 10$  m/day). 2D tank M (Experiment #6).

Fig. 6 shows the changes of gas volume over time in the tank, obtained by imaging. After a short delay, the gas volume decreased and reached a limit value corresponding to the remaining gas volume in the tank once all the strong foam is destroyed. It is interesting to note that the gas volume decreased little during the destruction of the strong foam (from 1150 mL to 955 mL). 83% of the gas supplied by the flow of foam, therefore, remains trapped in the porous medium, either at the initial location of the foam or above it by buoyancy. The photo of the tank after foam destruction shows a gas saturation distribution that is much more homogeneous than at the end of the injection. The tracing tests carried out at the end of the destruction of the foam show that the flow is slowed down in the foam injection zone but that it passes through this zone again (see Fig. 7).

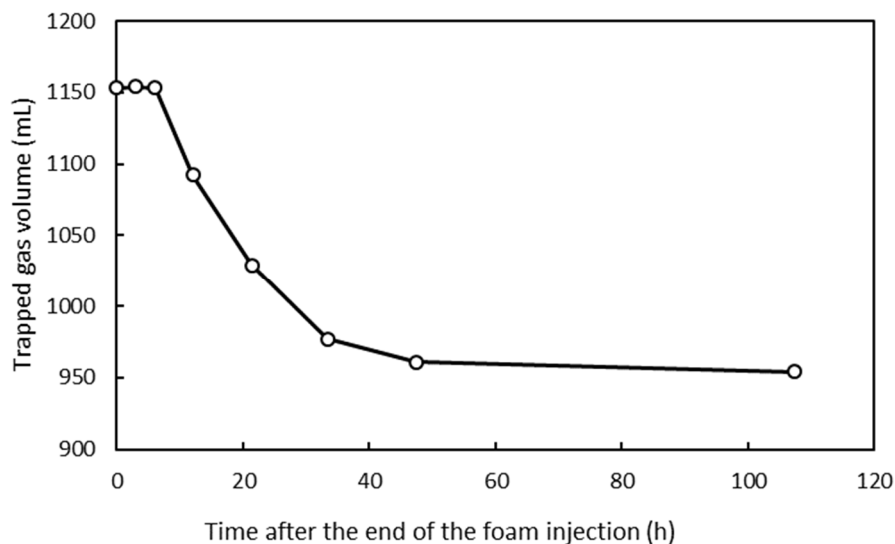


Fig. 6. How gas volume changes in the tank after the end of the injection. Tank M (Experiment #6).

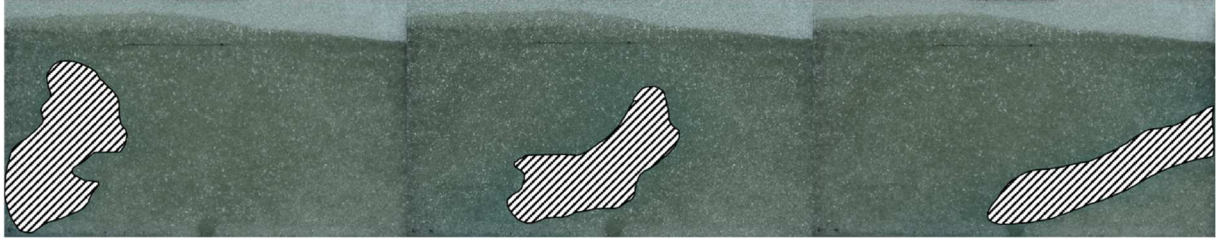


Fig. 7. Tracing after foam destruction. The tracer is identified by the hatched area (15 minutes between each photograph). Tank S (Experiment # 1).

The delay before the start of the destruction of the foam seems to be related to the surfactant concentration. Indeed, during the first moments of the stability phase, the surfactant solution is sufficiently concentrated to guarantee the stability of the foam. With the phenomenon of advection-diffusion at the interface, the concentration of surfactant in the solution decreases below the CMC, which promotes foam coalescence.

By taking photos, it is also possible to measure the height of the water in the inlet and outlet cavities. The height differences correspond to the pressure drop required to generate the lateral flow in the porous medium due to foam propagation in the pore space. This pressure drop corresponds to a reduction in the average mobility of water in the tank. This reduction can be presented as a resistance factor  $RF_{water,lat}(-)$  as below:

$$RF_{water,lat}(t) = \frac{\Delta h(t)}{\Delta h_{init}} \quad (6)$$

where  $\Delta h_{init}(m)$  is the difference in water height due to the lateral flow before the foam injection and  $\Delta h(m)$  is the difference in water height due to the lateral flow at time  $t$ .

The temporal evolution of resistance factor  $RF_{water,lat}$  is presented in Fig. 8 for experiment #6. During the foam injection phase, RF increases as gas was invading the tank. Water mobility is logically reduced because of the space occupied by the strong foam, which diverted the lateral flow. After stopping foam injection, RF continued to increase slowly compared to the foam injection stage. Consequently, water mobility continued to decrease despite the destruction of the strong foam because a large part of the gas supplied by the foam remained present in the tank. In addition, the gas that escaped from the strong foam, after foam coalescence, rose toward the surface and became trapped in pores. Thus, the gas saturation and its distribution increased in this zone above the strong foam and remained high in the zone previously occupied by the strong foam. Thus, the average mobility in the tank decreased during the coalescence of the strong foam.



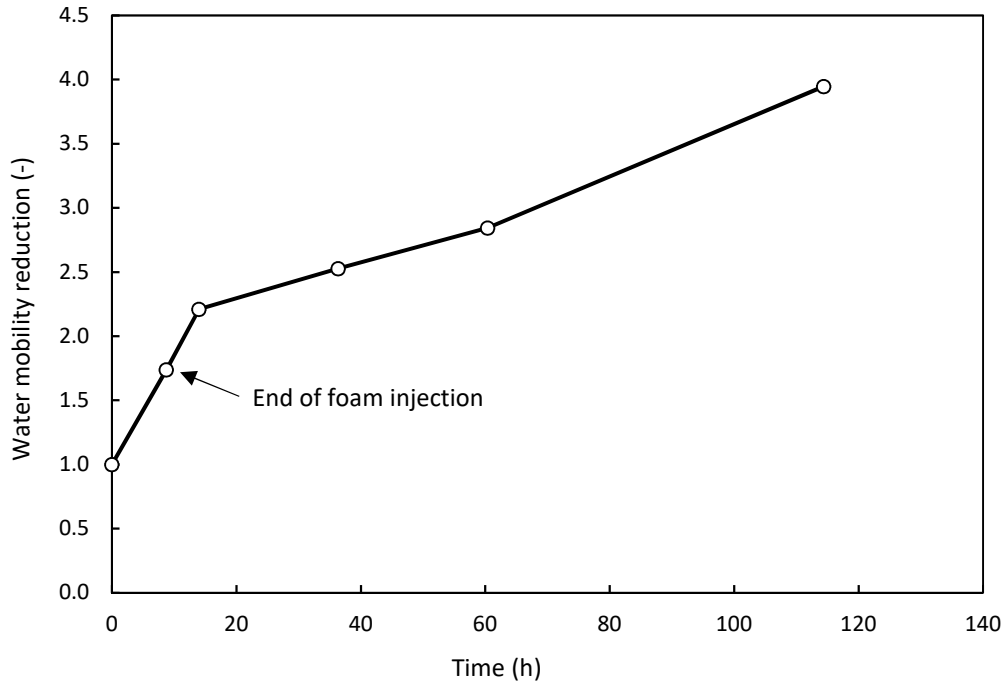


Fig. 8. Mobility reduction over time (Experiment #6).













Strong foam strictly diverts water flow during the injection phase but is gradually destroyed after the injection is stopped. After this destruction, the mobility of water greatly decreases due to the homogenization and distribution of gas saturation in the 2D tank. The lateral flow generates more pressure difference to flow into the tank after the foam is destroyed. Thus, the foam retains its blocking properties even after its destruction. The main interest of the foam for blocking an area could therefore be a means of transporting gas in a porous medium in a homogeneous manner thanks to its high viscosity. Once the zone is occupied by the foam, it can be destroyed to be replaced by the trapped gas, which will maintain a low relative permeability and can be trapped in pores for a longer time.

### 5.3. Influence of lateral flow type

To study how the type of lateral flow influenced foam propagation and stability, the injections were stopped at a time corresponding to the same water mass measured at the outlet of the tank to have the same gas saturation in the tank. After the foam injection was stopped, the lateral water flow was continued at the same velocity as during the injection. Fig. 9 shows the photos taken during the stability phase. Time zero corresponds to the end of the foam injection. Three different weak foam patterns were observed during the three types of flow at the end of foam injection ( $t=0$ ). These patterns were systematically observed for each of the

repetitions carried out under the same conditions. These photos were taken at equal trapped gas volumes for each experiment.

The main difference between open and closed flow was the presence of surfactant in the flowing water in the latter. Although the flow is the cause of unsymmetrical patterns in both cases, the surfactant supply in the closed flow contributes to the generation of a weak foam around the strong foam zone where gas and surfactant are present. The weak foam corresponds to gas bubbles, coming from the strong foam zone, that are stabilized by the surfactant molecules transported by the closed lateral flow. In the case without lateral flow, the strong foam is quickly destroyed and the gas coming from the strong foam zone is moving up in the tank.

t (h)	Open flow	Closed flow	Without flow
0			
24			
48			
72			

*Fig. 9. Influence of the type of flow (open flow: free surfactant water flow, closed flow: recirculating outlet flow, and without lateral flow) on the foam patterns during the stability phase. Time after the end of the injection.*

With an open flow, the strong foam is quickly destroyed. In contrast, the destruction of the foam is much more limited in the case of a closed flow. For an experiment without flow, only

a slight diffusion of the gas is observed, changing the strong foam contours slightly and without observing visible destruction. The absence of foam destruction for an experiment without lateral flow proves the fact that lateral flow is the main cause of the coalescence phenomena and therefore of the destruction of the strong foam. It is therefore concluded that it is the advection-diffusion phenomenon that dominates the coalescence dynamics of the strong foam. The experiments with the open and closed lateral flow were performed with the same lateral flow velocity and therefore exhibit the same viscous stresses on the strong foam. The fact that foam destruction was greatly reduced for closed flow proves that viscous interactions due to flow play a very limited role in foam destruction. The main advantage of using a closed flow is to supply the water flowing laterally with surfactant. The observed difference is therefore due to the presence of surfactant in the lateral flow. The closed circulation of water increases foam stability and reduces its rejection in groundwater.

#### 5.4. Influence of lateral flow velocity

Experiments were carried out in the M-tank to assess the influence of the lateral flow velocity. Four experiments (numbers 4, 5, 6, and 7) were carried out with lateral flow velocities of 5, 7.5, and 10 m/day and one experiment without any lateral flow. The results are presented below. To quantify the foam volume, the radius of influence (*ROI*) of the foam is defined as the geometric mean of the lateral radius  $R_h$  and the vertical radius  $R_v$  as  $ROI = \sqrt{R_h R_v}$ . To complete the analysis of the shape of the foam, the aspect ratio *AR* is defined as  $AR = R_h/R_v$ .

Only the shape of the strong foam zone will be discussed. Strong foam can be visually distinguished from weak foam and gas bubbles by the regularity of its shape as well as its color very close to white, indicating a high gas saturation. The areas of the tank where weak foam or gas bubbles flow have irregular shapes are difficult to qualify geometrically (Fig. 10).

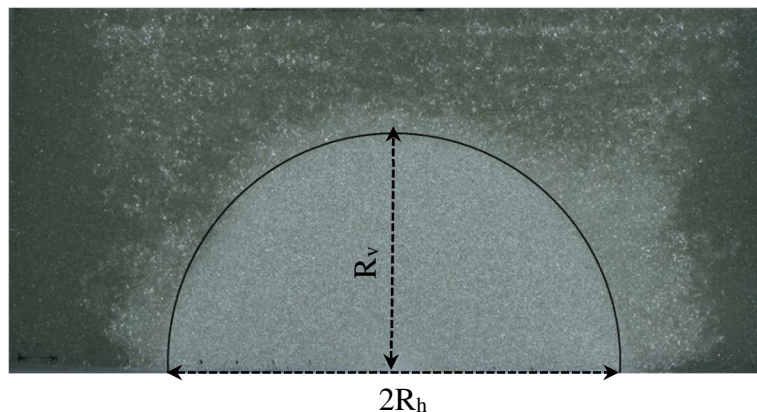


Fig. 10. Example of the form of foam propagation. The strong foam is visually identifiable by its white color and regular shape.

The results concerning the radius of influence are presented in Fig. 11 for different water lateral flow velocities. The dynamics of the radius of influence follow an evolution close to a power-law function. In the theoretical case where no coalescence phenomenon would occur, the radius of influence would evolve according to a relation of the type  $ROI = a\sqrt{t}$ , by geometric definition (for a constant the foam injection rate). The maximum theoretical value for  $a$  when the whole foam volume would be converted into strong foam can be calculated by  $a = \sqrt{\frac{2Q}{\phi\pi e}}$  with  $Q$  injection flow rate and  $\phi$  porous medium porosity.

However, because of the coalescence phenomena, part of the volume of injected gas escapes and is not included in the strong foam mass. Thus, the  $ROI$  follows a power law with an exponent less than 0.5 (0.44 - 0.47), depending on the coalescence rate.

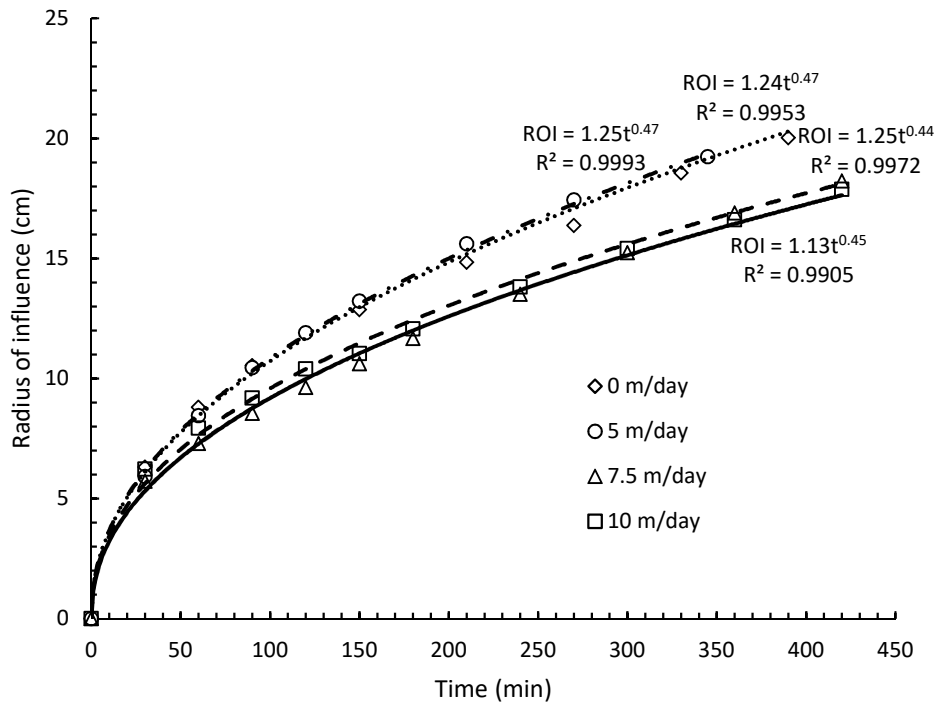


Fig. 11. Influence of the lateral flow velocity on the temporal evolution of the radius of influence.

The coalescence rate should be higher for higher lateral flow velocity; therefore, the exponent for the  $ROI$  factor is slightly lower. However, the precision of experiments does not allow us to see a significant difference between low lateral flow velocities (0 and 5 m/day) and high ones (7.5 and 10 m/day).

The aspect ratios are plotted in Fig. 12 for different water lateral flow velocities. The aspect ratios are just above 1 at the beginning of the injection and decrease with time to reach the

values closer to one at the end of the injection. The elongation observed in the horizontal direction at the beginning of the injection can be attributed to bottom wall effects. This means that the elongation of the half-ellipse is more horizontal at the beginning of the injection and tends to a half-circular form at the end. These results show that gravity has no significant impact on strong foam propagation. This confirms the results obtained in [Aranda et al., 2020], which show that in the case of the flow of a strong foam in a porous medium, the viscous forces are dominant over the gravitational forces. The lateral flow rate tends very slightly to increase the aspect ratio. However, because of the random pathway of foam (preferential paths) in the 2D tank, it is difficult to obtain more precise results.

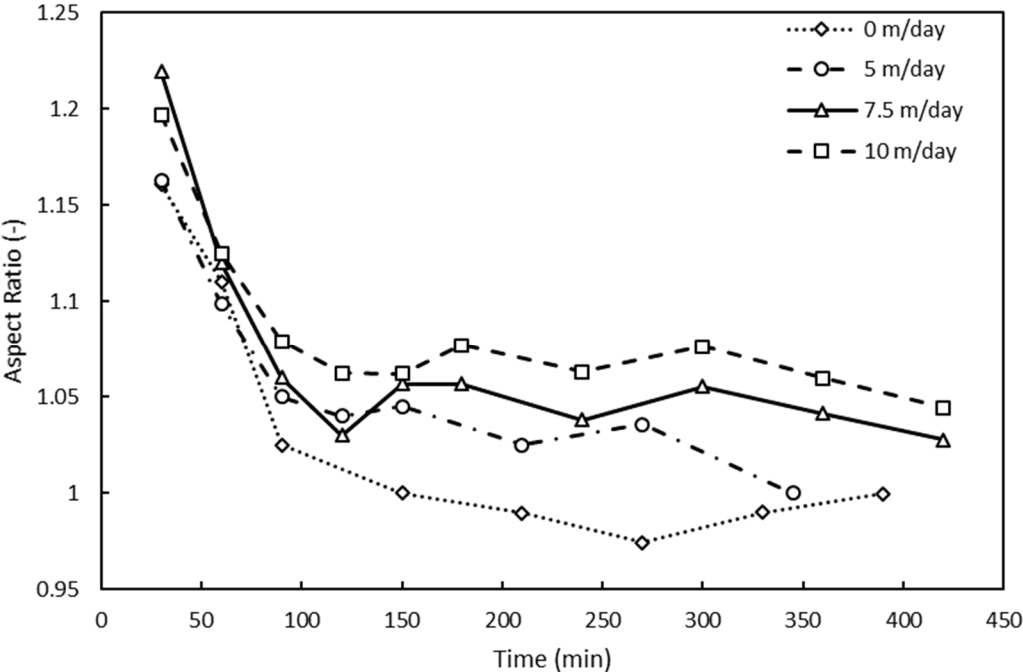
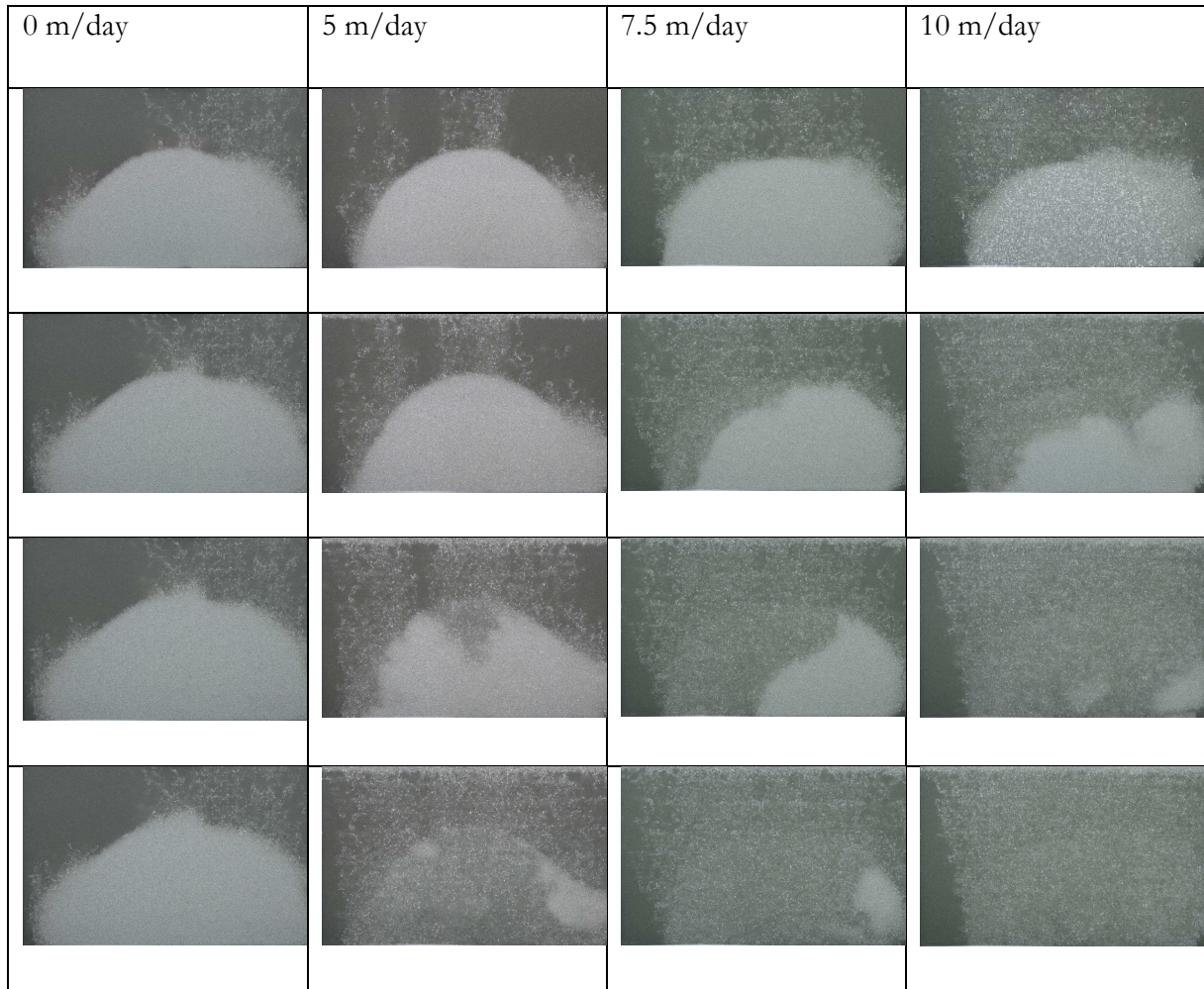


Fig. 12. Influence of lateral flow velocity on aspect ratio over time.

To study the influence of the lateral flow speed on the stability of the foam, the injections were stopped at the same mass measured at the outlet of the tank. After the foam injection was stopped, the lateral flow was continued at the same velocity as during the injection. Fig. 13 shows photos of the tanks, according to the time elapsed since the stopping of their respective foam injections. The lateral flow velocity has a significant impact on the stability of the strong foam. The higher the flow velocity, the faster the destruction of the strong foam. These observations support the hypothesis of destruction mainly controlled by dilution of the surfactant by lateral flow. The volumes of gas in the tank for each of the experiments were estimated by the imaging technique.



*Fig. 13. How foam patterns change during the stability phase for different flow velocities (Time step 20 hours).*

The results of these analyzes are presented in Fig. 14. Since the initial gas volumes vary slightly, the volumes are presented in the form of relative gas volume equal to the ratio between the gas volume at time  $t$  and the gas volume measured at the end of the injection ( $t=0$ ). The measurement error due to the difficulty to delimit the boundary between the strong foam zone and the exterior leads to values greater than 1 in the limit of 5%. For the 10 m/day experiment, the volume of gas remaining in the final state tank is quite high compared to the other experiments. However, the relevance of this graph lies in the destruction phase and not only on the value of the volume of gas in the final state.

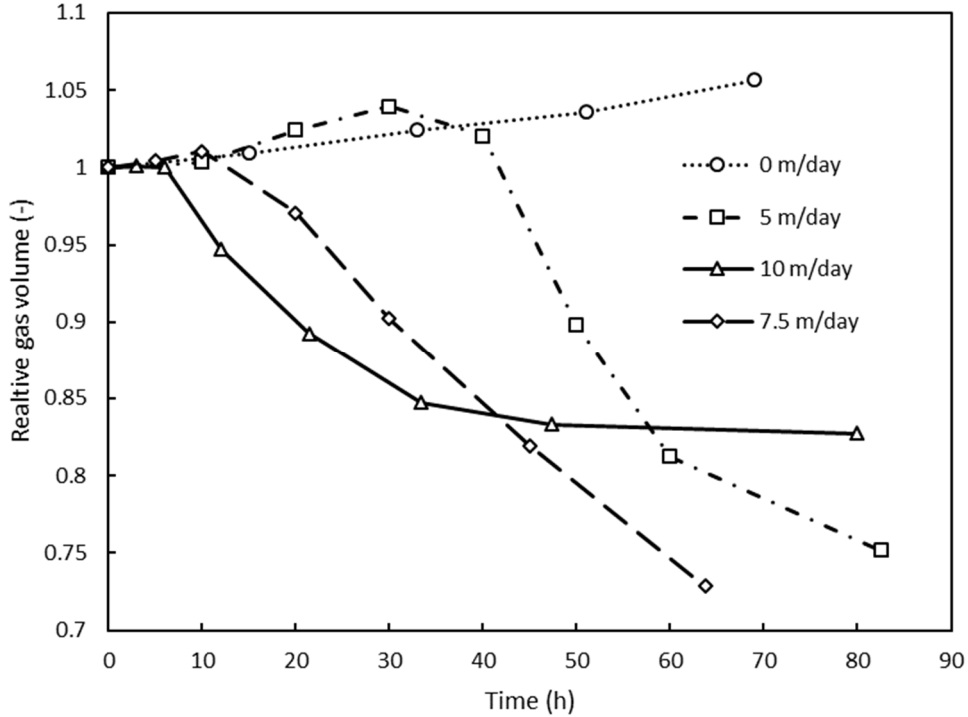


Fig. 14. Influence of lateral flow velocity on relative gas volume over time after the end of the injection.

First of all, in the absence of lateral flow, the foam zone is stable during the time of the experiment. In presence of lateral flow, the foam zone remains stable for a time that depends on the velocity. These times are around 30, 12, and 5 hours for 5, 7.5, and 10 m/day lateral water velocity, respectively. This delay is attributed to the time necessary to reduce the surfactant concentration below the CMC by an advection-diffusion phenomenon. The velocity of the flow primarily affects the time before decreasing the volume of gas. There is no significant difference in destruction speed between experiments after this time limit is reached. Since the advection and dispersion of surfactant are proportional to the velocity of the flow, the latter accelerates the loss of surfactant, and coalescence is initiated more quickly. When the surfactant concentration decreases, the strong foam coalesces starting with the areas with low surfactant concentration, i.e., the foam/water interface and in particular the sidewall on the upstream side of the lateral flow.

## 6. Conclusions

We studied the behavior of the foam flowing in a highly permeable porous medium in the presence of a lateral flow of water using 2D tank setups. The influence of this flow and its velocity on the propagation and stability of the foam have been studied in detail.

A flow of strong foam, in the form of a semi-circular semi-ellipse, and a weak foam around it followed by the free gas flow occurred during the foam injection. The quasi-circular shape of the strong foam shows its viscosity and the domination of viscous effects over gravity effects. The weak foam, on the other hand, flows toward the top of the tank, indicating a lower viscosity. Lateral flow creates an asymmetry in the weak foam pattern by inhibiting coalescence on the upstream side of the strong foam.

Tracing tests showed that all of the lateral flow was diverted by the strong foam during its injection thanks to its high viscosity. Stability tests have shown that all of the strong foam is destroyed within a few tens of hours. A low lateral flow rate helps to delay the onset of foam coalescence. We found that the coalescence is mainly controlled by the phenomenon of advection-diffusion of the surfactant in the 2D tank. It is expected that, when the surfactant concentration decreases below the critical micelle concentration (CMC), the strong foam begins to coalesce. Foam destruction decreases its viscosity and generates trapped and free-gas that escapes from the strong foam zone upwards towards the top of the tank. This increases gas saturation and its distribution in the area above the strong foam reducing water's mobility in the porous medium.

The foam, therefore, has a double blocking effect: the first is a strict and direct blocking effect caused by the viscosity of the strong foam, and the second is a relative and indirect blocking effect caused by the homogenous distribution of the gas phase in the porous medium. The gas remains trapped in the porous medium and slows the flows if these are generated by a constant pressure head as is the case with unconfined aquifers.

These results shed new light on the efficiency of foam as a blocking agent, showing that it can also serve as a means of transporting gas more efficiently in porous media, especially for soil remediation applications.

## **7. Acknowledgments**

This study was performed as part of the “Famous” project. The authors would like to thank ADEME for co-funding the project under the GESIPOL program and BRGM/DEPA and Solvay France for providing the Ph.D. grant for Romain Aranda. We gratefully acknowledge the financial support provided to the PIVOTS project by the “Région Centre – Val de Loire” and the European Regional Development Fund.



## 8. References

- [Alazaiza et al., 2016] Alazaiza, M. Y. D., Ngien, S. K., Ishak, W. M. F. and Kamaruddin, S. A.: 2016, A review of light reflection and transmission methods in monitoring non-aqueous phase liquid migration in porous media., *ARPJ Journal of Engineering and Applied Science* **11**(4), 2319–2326.
- [Aranda et al., 2020] Aranda, R., Davarzani, H., Colombano, S., Laurent, F. and Bertin, H.: 2020, Experimental study of foam flow in highly permeable porous media for soil remediation, *Transport in Porous Media* **134**(1), 231–247. <https://doi.org/10.1007/s11242-020-01443-8>
- [Bertin et al., 2017] Bertin, H., Del Campo Estrada, E. and Atteia, O.: 2017, Foam placement for soil remediation, *Environ. Chem.* **14**(5), 338–343. <https://doi.org/10.1071/EN17003>
- [Bouزيد et al., 2018] Bouزيد, I., Maire, J., Ahmed, S. I. and Fatin-Rouge, N.: 2018, Enhanced remedial reagents delivery in unsaturated anisotropic soils using surfactant foam, *Chemosphere* **210**, 977–986.
- [Câdík, 2008] Câdík, M.: 2008, Perceptual evaluation of color-to-grayscale image conversions, *Computer Graphics Forum* **27**(7), 1745–1754. <https://onlinelibrary.wiley.com/doi/abs/10.1111/j.1467-8659.2008.01319.x>
- [Choi et al., 2009] Choi, Y. J., Kim, Y.-J. and Nam, K.: 2009, Enhancement of aerobic biodegradation in an oxygen-limiting environment using a saponin-based microbubble suspension, *Environmental Pollution* **157**(8), 2197–2202. <https://www.sciencedirect.com/science/article/pii/S0269749109002073>
- [Colombano et al., 2020] Colombano, S., Davarzani, H., van Hullebusch, E., Huguenot, D., Guyonnet, D., Deparis, J. and Ignatiadis, I.: 2020, Thermal and chemical enhanced recovery of heavy chlorinated organic compounds in saturated porous media: 1d cell drainage-imbibition experiments, *Science of The Total Environment* **706**, 135758. <https://www.sciencedirect.com/science/article/pii/S0048969719357535>
- [Couto et al., 2009] Couto, H. J., Massarani, G., Biscaia, E. C. and Sant'Anna, G. L.: 2009, Remediation of sandy soils using surfactant solutions and foams, *Journal of Hazardous Materials* **164**(2), 1325–1334.

<https://www.sciencedirect.com/science/article/pii/S0304389408013848>

[Dicksen et al., 2002] Dicksen, T., Hirasaki, G. J. and Miller, C. A.: 2002, Mobility of Foam in Heterogeneous Media: Flow Parallel and Perpendicular to Stratification, *SPE Journal* **7**(02), 203–212. <https://doi.org/10.2118/78601-PA>

[Flores et al., 2011] Flores, G., Katsumi, T., Inui, T. and Kamon, M.: 2011, A simplified image analysis method to study Inapl migration in porous media, *Soils and Foundations* **51**(5), 835–847.

[Forey et al., 2021] Forey, N., Atteia, O., Omari, A. and Bertin, H.: 2021, Use of saponin foam reinforced with colloidal particles as an application to soil remediation: Experiments in a 2d tank, *Journal of Contaminant Hydrology* **238**, 103761. <https://www.sciencedirect.com/science/article/pii/S0169772220303508>

[Géraud et al., 2017] Géraud, B., Méheust, Y., Cantat, I. and Dollet, B.: 2017, Lamella division in a foam flowing through a two-dimensional porous medium: A model fragmentation process, *Phys. Rev. Lett.* **118**, 098003.

<https://link.aps.org/doi/10.1103/PhysRevLett.118.098003>

[Jeong and Corapcioglu, 2003] Jeong, S.-W. and Corapcioglu, M. Y.: 2003, A micromodel analysis of factors influencing napl removal by surfactant foam flooding, *Journal of contaminant hydrology* **60**(1), 77–96.

[Jeong et al., 2000] Jeong, S.-W., Corapcioglu, M. Y. and Roosevelt, S. E.: 2000, Micromodel study of surfactant foam remediation of residual trichloroethylene, *Environmental science & technology* **34**(16), 3456–3461.

[Kechavarzi et al., 2000] Kechavarzi, C., Soga, K. and Wiart, P.: 2000, Multispectral image analysis method to determine dynamic fluid saturation distribution in two-dimensional three-fluid phase flow laboratory experiments, *Journal of Contaminant Hydrology* **46**(3), 265–293. <https://www.sciencedirect.com/science/article/pii/S0169772200001339>

[Khatib et al., 1988] Khatib, Z., Hirasaki, G. and Falls, A.: 1988, Effects of Capillary Pressure on Coalescence and Phase Mobilities in Foams Flowing Through Porous Media, *SPE Reservoir Engineering* **3**(03), 919–926. <https://doi.org/10.2118/15442-PA>

[Kovscek and Bertin, 2003] Kovscek, A. R. and Bertin, H. J.: 2003, Foam mobility in heterogeneous porous media, *Transport in Porous Media* **52**(1), 37–49. <https://doi.org/10.1023/A:1022368228594>

[Kovscek et al., 2007] Kovscek, A., Tang, G.-Q. and Radke, C.: 2007, Verification of roof snap off as a foam-generation mechanism in porous media at steady state, *Colloids and Surfaces A: Physicochemical and Engineering Aspects* **302**(1), 251–260. <https://www.sciencedirect.com/science/article/pii/S0927775707001501>

[Longpré-Girard et al., 2016] Longpré-Girard, M., Martel, R., Robert, T., Lefebvre, R. and Lauzon, J.-M.: 2016, 2d sandbox experiments of surfactant foams for mobility control and enhanced Inapl recovery in layered soils, *Journal of Contaminant Hydrology* **193**, 63–73. <https://www.sciencedirect.com/science/article/pii/S0169772216301826>

[Luciano et al., 2010] Luciano, A., Viotti, P. and Papini, M. P.: 2010, Laboratory investigation of DNAPL migration in porous media, *Journal of Hazardous Materials* **176**(1), 1006–1017. <https://www.sciencedirect.com/science/article/pii/S030438940901961X>

[Maire et al., 2019] Maire, J., Davarzani, H., Colombano, S. and Fatin-Rouge, N.: 2019, Targeted delivery of hydrogen for the bioremediation of aquifers contaminated by dissolved chlorinated compounds, *Environmental Pollution* **249**, 443–452. <https://www.sciencedirect.com/science/article/pii/S026974911834260X>

[Mulligan and Eftekhari, 2003] Mulligan, C. N. and Eftekhari, F.: 2003, Remediation with surfactant foam of PCP-contaminated soil, *Engineering Geology* **70**(3), 269–279. Third British Geotechnical Society Geoenvironmental Engineering Conference. <https://www.sciencedirect.com/science/article/pii/S0013795203000954>

[O'Carroll et al., 2004] O'Carroll, D. M., Bradford, S. A. and Abriola, L. M.: 2004, Infiltration of PCE in a system containing spatial wettability variations, *Journal of Contaminant Hydrology* **73**(1), 39–63.

<https://www.sciencedirect.com/science/article/pii/S0169772203002584>

[Omirebekov et al., 2020a] Omirebekov, S., Davarzani, H. and Ahmadi-Senichault, A.: 2020a, Experimental study of non-Newtonian behavior of foam flow in highly permeable porous media, *Industrial & Engineering Chemistry Research* **59**(27), 12568–12579. <https://doi.org/10.1021/acs.iecr.0c00879>

[Omirebekov et al., 2020b] Omirebekov, S., Davarzani, H., Colombano, S. and Ahmadi-Senichault, A.: 2020b, Experimental and numerical upscaling of foam flow in highly permeable porous media, *Advances in Water Resources* **146**, 103761. <https://www.sciencedirect.com/science/article/pii/S0309170820302074>

[Philippe et al., 2020] Philippe, N., Davarzani, H., Colombano, S., Dierick, M., Klein, P.-Y. and Marcoux, M.: 2020, Experimental study of the temperature effect on two-phase flow properties in highly permeable porous media: Application to the remediation of dense non-aqueous phase liquids (DNAPLs) in polluted soil, *Advances in Water Resources* **146**, 103783. <https://www.sciencedirect.com/science/article/pii/S0309170820301652>

[Portois et al., 2018a] Portois, C., Boeije, C. S., Bertin, H. J. and Atteia, O.: 2018a, Foam for environmental remediation: Generation and blocking effect, *Transport in Porous Media* **124**(3), 787–801. <https://doi.org/10.1007/s11242-018-1097-z>

[Portois et al., 2018b] Portois, C., Essouayed, E., Annable, M. D., Guiserix, N., Joubert, A. and Atteia, O.: 2018b, Field demonstration of foam injection to confine a chlorinated solvent source zone, *Journal of Contaminant Hydrology* **214**, 16–23. <https://www.sciencedirect.com/science/article/pii/S0169772217303728>

[Rossen et al., 1999] Rossen, W., Zeilinger, S., Shi, J. and Lim, M.: 1999, Simplified Mechanistic Simulation of Foam Processes in Porous Media, *SPE Journal* **4**(03), 279–287. <https://doi.org/10.2118/57678-PA>

[Rothmel et al., 1998] Rothmel, R. K., Peters, R. W., St. Martin, E. and DeFlaun, M. F.: 1998, Surfactant foam/bioaugmentation technology for in situ treatment of TCE-DNAPLs, *Environmental Science & Technology* **32**(11), 1667–1675. <https://doi.org/10.1021/es970980w>

[Schincariol et al., 1993] Schincariol, R. A., Herderick, E. E. and Schwartz, F. W.: 1993, On the application of image analysis to determine concentration distributions in laboratory experiments, *Journal of Contaminant Hydrology* **12**(3), 197–215. <https://www.sciencedirect.com/science/article/pii/016977229390007F>

[Sheng, 2013] Sheng, J.: 2013, *Enhanced Oil Recovery Field Case Studies*, Gulf Professional Publishing.

[Wang and Mulligan, 2004] Wang, S. and Mulligan, C. N.: 2004, An evaluation of surfactant foam technology in remediation of contaminated soil, *Chemosphere* **57**(9), 1079–1089. <http://www.sciencedirect.com/science/article/pii/S0045653504006964>

[Wever et al., 2011] Wever, D., Picchioni, F. and Broekhuis, A.: 2011, Polymers for enhanced oil recovery: A paradigm for structure-property relationship in aqueous solution, *Progress in Polymer Science* **36**(11), 1558–1628. Special Topic: Energy Related Materials. <https://www.sciencedirect.com/science/article/pii/S0079670011000682>

[Zhong et al., 2011] Zhong, L., Szecsody, J., Oostrom, M., Truex, M., Shen, X. and Li, X.: 2011, Enhanced remedial amendment delivery to subsurface using shear thinning fluid and aqueous foam, *Journal of Hazardous Materials* **191**(1-3), 249–257.